Süleyman Demirel Üniversitesi
Fen Bilimleri Enstitüsü Dergisi
Cilt 25, Sayı 1, 64-73, 2021

Süleyman Demirel University
Journal of Natural and Applied Sciences
Volume 25, Issue 1, 64-73, 2021

DOI: 10.19113/sdufenbed.801973

# Molecular Dynamics and MM-PBSA Studies for Deciphering Molecular Interactions of Valproic Acid with CYP2C9 Mutants F114L and I207T

**Ahmet Can TİMUÇİN**[*1]

[1]Üsküdar University, Faculty of Engineering and Natural Sciences, Department of Chemical Engineering, 34662, İstanbul, Turkey

(Alınış / Received: 30.09.2020, Kabul / Accepted: 25.01.2021, Online Yayınlanma / Published Online: 15.04.2021)

**Keywords**
CYP2C9,
MD simulations,
MM-PBSA,
Valproic acid

**Abstract:** Valproic Acid (VPA) is a widely used drug, particularly in neuropsychiatric disorders, while showing promise in other types of diseases such as cancer. VPA metabolism via cytochrome P450 (CYP) pathway is responsible from only ~10% of the total drug dose. However, due to high risk of severe adverse reactions in liver and pancreas, interaction of VPA with CYP2C9 remains to be delineated chiefly in CYP2C9 mutants. Hence, here we implemented a molecular dynamics study, followed by MM-PBSA (Molecular Mechanics Poisson-Boltzmann Surface Area) method based relative binding energy estimation to understand how F114L and I207T CYP2C9 mutants changed their binding mode towards VPA in comparison to wild type (WT) CYP2C9. Results indicated that while F114L and I207T mutants have showed significant decrease in total relative binding energy, compared with WT, there were a clear shift of occupied amino acids responsible for VPA interaction in mutants vs WT. Overall, here for the first time in literature, this novel shift of VPA interacting amino acids in F114L and I207T mutants were reported. Limitations and future perspective of the data were also discussed.

# Valproik Asit ile CYP2C9 Mutantları F114L ve I207T Moleküler Etkileşimlerinin Çözümlenmesi için Moleküler Dinamik ve MM-PBSA Çalışmaları

**Anahtar Kelimeler**
CYP2C9,
MD simulasyonları,
MM-PBSA,
Valproik asit

**Özet:** Valproik asit (VPA), özellikle nöropsikiyatrik bozukluklarda kullanılan bir ilaç olup, kanser gibi diğer tip hastalıklarda da umut vaat etmektedir. Sitokrom P450 (CYP) yolağı tarafından gerçekleştirilen VPA metabolizması toplam ilaç dozunun sadece %10 kadarıdır. Ancak, karaciğer ve pankreasta şiddetli yan etki reaksiyonları gösterme riski yüksek olduğu için, VPA`nın CYP2C9 ile ve özellikle CYP2C9 mutantları ile nasıl etkileştiği açıklanmayı beklemektedir. Bu nedenle, biz burada moleküler dinamik çalışmaları ve devamında yapılan MM-PBSA (Moleküler Mekanik Poisson-Boltzmann Yüzey Alanı) metodu tabanlı bağıl bağlanma enerjisi tahmini ile CYP2C9 mutantları F114L ve I207T`nin VPA ile bağlanma modunun doğal fenotipli (WT) CYP2C9`a göre nasıl değiştiğini anlamayı amaçladık. Sonuçlar, F114L ve I207T mutantlarının toplam bağıl bağlanma enerjilerinin doğal fenotipe göre önemli miktarda düştüğünü göstermiş olup, ayrıca mutantların VPA etkileşimi için kullandıkları amino asitlerde de, doğal fenotipe göre net bir değişim olduğunu ortaya koymuştur. Tümde, literatürde bir ilk olarak, VPA ile etkileşen amino asitlerdeki bu özgün değişim raporlanmıştır. Verilerin kısıtlamaları ve gelecek perspektifi de ayrıca tartışılmıştır.

## 1. Introduction

VPA is a branched short chain fatty acid, mainly used for treating epilepsy, migraine and other psychiatric conditions [1, 2]. VPA as a molecule capable of inhibiting histone deacetylases, has also been under investigation towards cancer, HIV and other neurodegeneration related disorders [2, 3]. When VPA is administered, ~90% of the total dose remains protein bound [2, 4]. Apart from glucuronidation and β oxidation based mitochondrial metabolism, CYP dependent oxidation holds ~10% of the overall VPA

*Corresponding author: ahmetcan.timucin@uskudar.edu.tr

metabolism [2, 5-7]. CYP2C9 and CYP2A6 were known to be the main metabolizers of VPA converting it to 4-ene VPA, 4-OH VPA and 5-OH VPA [2, 8-10]. While only ~10% of VPA metabolism was known to be accomplished by CYPs, VPA was also linked to critical adverse reactions in liver, pancreas and was reported to be teratogenic [1, 2]. Thus, understanding how different mutations alter enzymatic activity of CYPs remains as a question to be deciphered, which prompted this study.

CYPs are oxidase-dehydrogenase enzymes, containing a buried heme group complexed with a cysteine [11]. Among these, CYP2C9 was known to be responsible from metabolism %15 of the drugs that are destined to CYP based transformation [12, 13]. In a study that excluded individuals with poor CYP metabolism and analyzed only healthy individuals, CYP2C9 protein content and activity was shown to be prone to high variability, indicating further studies are necessary to understand how different CYP2C9 alleles behave towards different ligands [12, 14, 15]. Hence, here a computational approach was taken to delineate how F114L and I207T mutations alter VPA binding to CYP2C9 through comparing them to WT CYP2C9.

Current literature contains only one molecular dynamics study analyzing VPA and WT CYP2C9 in terms of binding energetics and average structure based amino acid contributions [11]. Here, with our study, for the first time in literature, F114L and I207T mutants were analyzed relative to WT CYP2C9 via molecular dynamics and MM-PBSA method to reveal binding energetics and binding energy based amino acid contributions to VPA binding. More specifically, WT CYP2C9, as well as its mutant structures were first subjected to molecular docking studies to dock VPA in active sites of the structures. These structures were then used for 50 ns long molecular dynamics studies, which was followed by MM-PBSA based prediction of relative binding energies between CYP2C9 and VPA. Estimation of relative binding energy was further used for detailed analyses of amino acid-wise contributions to VPA binding. Obtained data was also validated by distance analyses and change in the total number of hydrogen bonds between VPA and selected key residues of CYP2C9. Overall, a novel shift of occupied amino acids responsible for VPA binding to enzymatic active site of mutant CYP2C9s in comparison to WT CYP2C9 were revealed. Moreover, results were also discussed in terms of limitations and possible future studies.

## 2. Material and Method

### 2.1. Molecular docking

The crystal structure of CYP2C9 (PDB ID: 1R9O) was used for molecular docking of VPA into CYP2C9 enzymatic pocket. Since this structure contained flurbiprofen in its enzymatic active site, it was removed prior to docking. Heme was kept in the original coordinates found in the crystal structure. Missing residues were completed using Modeller [16]. F114L and I207 mutants of CYP2C9 were generated via mutator plugin 1.3 of visual molecular dynamics (VMD) software [17]. The active site was defined using residues F114 and I207. All the docking studies were implemented using Autodock Vina [18].

### 2.2. Molecular dynamics studies

Topology and parameters for VPA were retrieved using CGenFF software [19, 20]. At the first step, all the WT and mutant complexes, including heme and VPA, were solvated in water and neutralized with NaCl. Simulations were completed via NAMD software using CHARMM parameters [21-24]. Explicit treatment of water molecules was completed using TIP3P model [25]. In all simulations, NPT ensemble was used together with periodic boundary conditions. Coulomb interactions were computed using particle-mesh Ewald algorithm. 15 Å limit was used for computing non-bonded electrostatic and Van der Waals interactions. Pressure was kept at 1 atm via Nosé−Hoover Langevin method and temperature was kept at 310K using Langevin dynamics [26, 27]. Lengths of the hydrogen-containing bonds were constrained using SHAKE algorithm [28]. Coordinates were recorded each 25 ps. All systems were first energy minimized via conjugate gradient method in 20000 steps. Second, temperature of each system was raised from 20 K to 310 K in 5 ps. Following heating step, all systems were equilibrated in 10 ns without any restraints on any atoms. This was followed by production runs of total 50 ns. WT production simulations were repeated twice whereas mutants were produced in triplicates. Total production run of 400 ns was analyzed. All molecular dynamics simulations and calculations were completed using TÜBİTAK TRUBA infrastructure. After production runs, trajectories were analyzed by Visual Molecular Dynamics (VMD) [17]. RMSD (Root mean square displacement) of backbone atoms were used to assess convergence of conformational stabilities. RMSF (Root mean square fluctuations) analyses was used to evaluate flexibility of VPA atoms in different simulations. Distance analyses was conducted to analyze if VPA was held in close vicinity to some MM-PBSA selected CYP2C9 enzymatic active residues. Ligplot+ analyses were conducted to analyze hydrogen bonding and hydrophobic contacts at 50$^{th}$ ns of MD simulations [29]. Total hydrogen bonding was also assessed to follow any temporal changes were present in this type of bonding between WT and mutant CYP2C9 simulations.

### 2.3. Prediction of relative binding energy between CYP2C9 and VPA using MM-PBSA method

As previously performed between WT CYP2C9 and VPA, MM-PBSA method was used to estimate relative

binding energy between CYP2C9 and VPA both in WT and mutant structures [11]. Final 10 ns of the 50 ns production runs were utilized for prediction of relative binding energies. During MM-PBSA calculations, internal dielectric constant was set to ε=1 and external dielectric constant was set to ε=80. 25 snapshots extracted from final 10 ns of each trajectory were used for predictions. MM-PBSA.py of Ambertools was employed for estimation of relative binding energies and contribution of amino acid to the calculated binding energy [30].

### 2.4. Statistical analyses

Data were expressed as mean ± SEM. Where appropriate, statistical significance was evaluated using student`s t-test. Statistical significance was defined using p value < 0.05.

## 3. Results

In order to delineate dynamically important amino acids involved in VPA binding to CYP2C9 active site, initial step of the study involved structure preparation of WT CYP2C9 and its selected mutants. Accordingly, at the first phase of this study, structure of human cytochrome P450 2C9 (CYP2C9) was retrieved from protein data bank [31, 32] (PDB ID: 1R9O). This structure contained flurbiprofen in its active site as well as heme which were removed prior to introduction of mutations. After ligand and cofactor removal procedure, missing residues were added to the wild type protein chain. The completed wildtype structure of CYP2C9 (CYP2C9*1) was then subjected to amino acid replacements to generate F114L (Phe114Leu) and I207T (Ile207Tyr) (CYP2C9*48) mutants [33]. At this point, man-made synthetic F114L mutant [34] was generated since F114 was a well-established residue for ligand binding of VPA [11]. Moreover, I207T mutant was preferred due to its close position in the active site to the other ligand binding residues (Figure 1) and due to prior information on diminished activity of I207T mutant of CYP2C9 towards diclofenac [33]. The positions of the mutated residues together with other important amino acids were depicted in Figure 1.

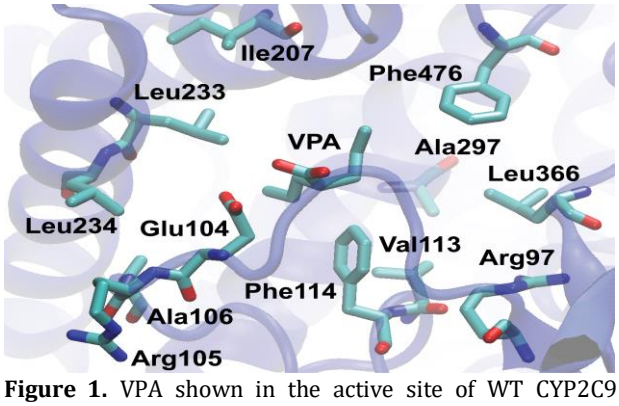


**Figure 1.** VPA shown in the active site of WT CYP2C9 together with key residues identified in this study (PDB ID: 1R9O).

Next, WT, F114L and I207T CYP2C9 structures were subjected to small ligand docking procedure to dock VPA into enzymatic active site of these structures. The results of the docking procedure was presented in the Figure 1 for the WT structure. Moreover, heme was also replaced into its original coordinates found in the initially obtained crystal structure (PDB ID: 1R9O), following VPA docking. After docking, all of the structures were used to implement production runs, composed of 50 ns MD simulations.

The first step taken in the analyses of 50 ns MD simulations was assessment of backbone RMSD based conformational stability (Figure 2A, 2B and 2C). These analyses yielded that all of the simulations returned less than 3 Å of RMSD fluctuations during the last 40 ns of the MD simulations (Figure 2A, 2B and 2C), which was a signature of conformational stability. This led us to use those stable frames of the simulations for more detailed analyses.

Following determination of conformational stability, last 10 ns of the stable final 40 ns of each MD simulations were used for estimation of relative binding energy between VPA vs. WT and mutant CYP2C9 structures. These predictions were the key step of this study since it allowed us to dissect the individual contributions of amino acid residues important for interactions in each case. Through comparing wild type and mutant amino acid contributions to the relative binding energy between VPA and CYP2C9 structures, molecular maps of perturbed inter-molecular interactions were aimed to be established. The first step in analyses of binding energies was the comparison of total interaction energy between WT and mutant complexes, which had returned statistically significant decreases upon both mutations, F114L and I207T (Figure 3A). When contributions of amino acids to the relative binding energy were analyzed between WT and mutant complexes, there was clear shift in both mutants in terms of utilization of amino acids. While WT structure was using the amino acids network composed of Glu104, Arg105 and Ala106 together with Leu233 and Leu234 for VPA interaction, F114 and I207T almost completely lost this network (Figure 3B). Instead, the mutant complexes shift to two new networks of which F114L used Arg97 and Val113, and I207T utilized Val113, Ala297, Leu266 and Phe476 for VPA interaction (Figure 3B). Moreover, individual contributions of heme and VPA have shown decreased level of contributions to the relative binding energy between mutant proteins and VPA, once again validating the shifted amino acid network, leading to diminished interaction level in mutants (Figure 3C). Altogether, these observations clearly indicated MM-PBSA based analysis of relative binding energy between enzyme and VPA together with analyses of residue wise contributions residue could be used as a predictor of diminished enzymatic activity of these mutants.

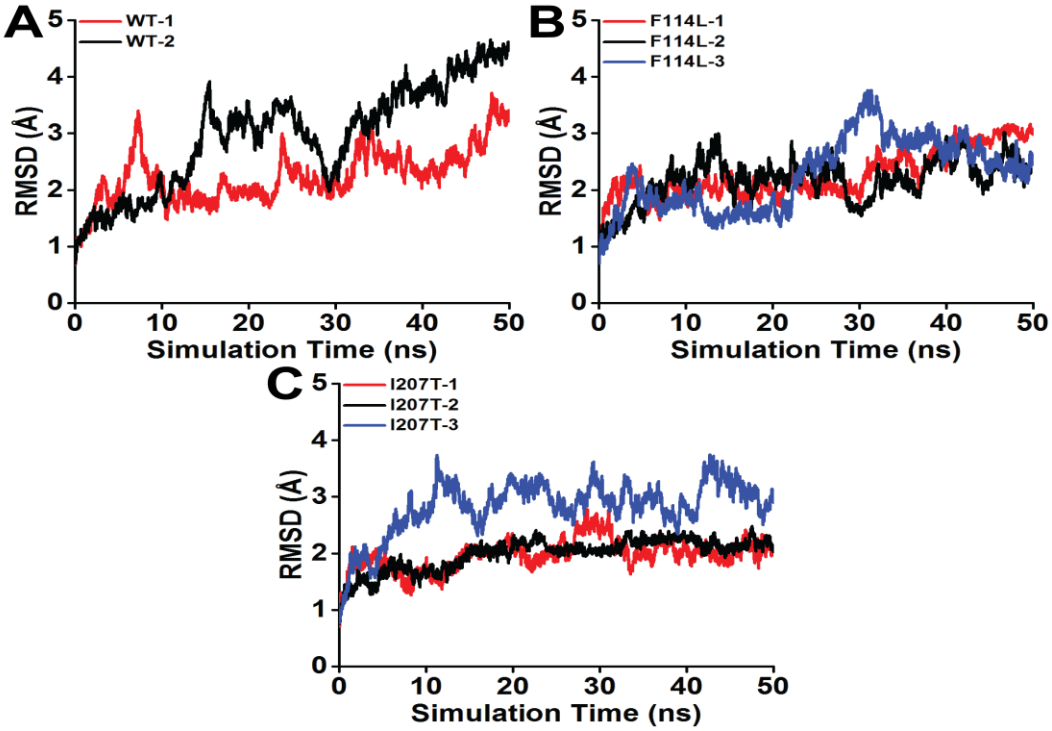


**Figure 2.** Backbone RMSD based conformational stability analyses of wildtype (WT) CYP2C9 (A) and its mutants F114L (B) and I270T (C) for 50 ns of MD simulations. All the systems analyzed contained VPA (Valproic acid) in their active sites together with heme cofactor. Results indicated that simulations have reached conformational stability after first 10 ns of MD simulations illustrated through less than ~3 Å of RMSD fluctuations. WT simulations were repeated in duplicates, whereas mutants were produced in triplicates

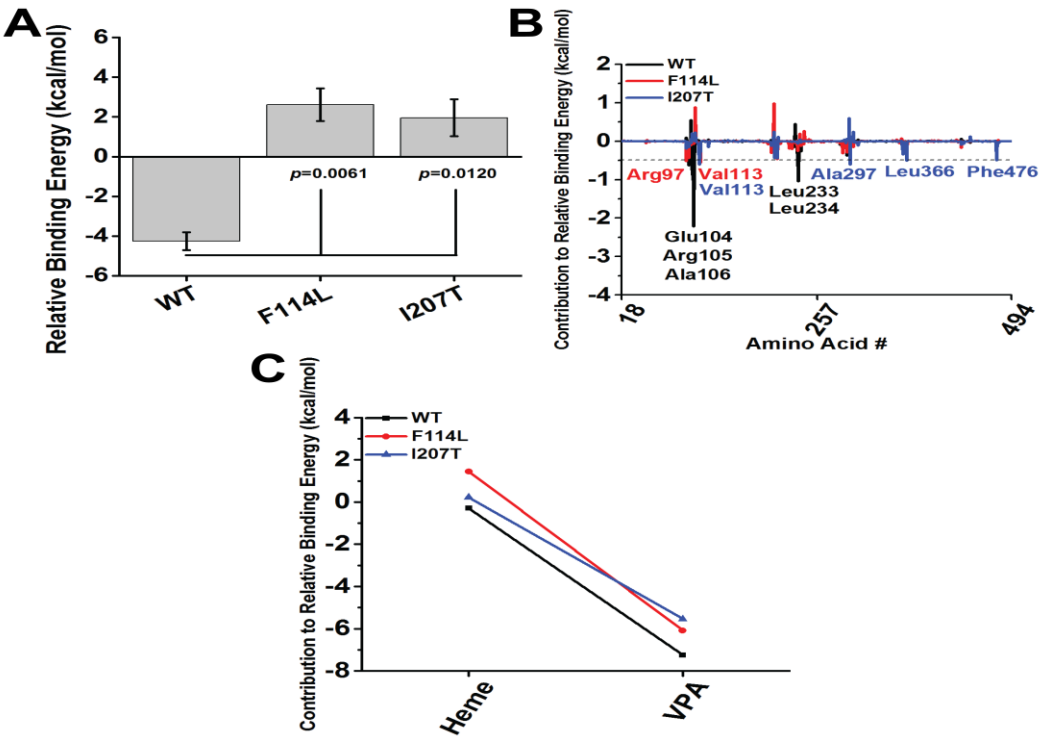


**Figure 3.** (A) VPA had shown significantly higher relative binding energy towards WT CYP2C9, compared with F114L and I207T mutants ($p<0.05$). Components of these interaction energies were shown in Table 1. (B) Contributions of WT and mutant CYP2C9 amino acids to the relative binding energy towards VPA were presented. WT CYP2C9 has shown utilization of Glu104, Arg105 and Ala106 together with Leu233 and Leu234, during its interaction with VPA. On the other hand, F114L mutant of CYP2C9 lost all the WT interactions, but continued to interact with VPA via contribution of the two amino acids, Arg97 and Val113. Furthermore, I207T of CYP2C9, similar to F114L mutant, lost all the interactions shown in WT but gained another network of amino acids, Val113, Ala 297, Leu266 and Phe476 for interacting VPA. Dashed line represents threshold selected for choosing amino acid (<-0.5 kcal/mol) in (B). (C) The individual contributions of heme and VPA to the relative binding energy towards WT and CYP2C9 mutants were shown. Both of the heme and VPA had less contributions to the relative binding energy in mutants compared to the WT complex.

Following identification of amino acid wise contributions, total interaction energy between VPA vs WT and mutant CYP2C9 molecules were investigated in terms of their components. All the complexes had shown positive total solvation energies (ΔG (Solvation)) indicating they were not favorable (Table 1). However, total gas phase molecular mechanics energy (ΔG (Gas)) of WT-VPA complex compensated for the numerically positive solvation energy, leading to -4.3 kcal/mol of interaction energy (Table 1). Compensation of solvation energy via gas phase molecular mechanics energy were not found in neither of the mutants (Table 1). When the sum of total polar contributions (ΔE (EEL) + ΔE (EPB)) were analyzed for WT and mutant binding energies, all contributions remained numerically positive, indicating unfavorable polar contribution to relative binding energy in all complexes (+7.5 kcal/mol for WT, +8.5 kcal/mol for F114L, + 9.0 kcal/mol for I207T) (Table 1). On the other side, when total non-polar contributions (ΔE (VDWAALS) + ΔE (ENPOLAR) + ΔE (EDISPER)) were analyzed, WT-VPA complex had shown a clear ∼2 fold increase compared to both mutants (-11.7 kcal/mol for WT, -5.9 kcal/mol for F114L, -6.9 kcal/mol for I207T) (Table 1). Overall, it was evident that non-polar interactions were the main contributor to the relative binding energy between VPA and WT CYP2C9 active site. However, loss of total non-polar contribution yielded numerically positive, thus unfavorable relative binding energies in the mutants.

In order to validate MM-PBSA based observations, next, distance analyses were implemented in between center of mass of selected key residues and center of mass of VPA (Figure 4A). It was evident that those key amino acid residues identified at the last 10 ns of MD simulation through MM-PBSA method, Arg105 and Leu234 of WT CYP2C9 remained almost 2 fold closer to VPA during last 40 ns of MD simulations, compared with mutants (Figure 4A). Hence, it was concluded that distance based observations for last 40 ns were confirmatory of MM-PBSA based estimation of relative binding energy, calculated for the last 10 ns. Furthermore, average RMSF based flexibility analyses of VPA molecules in WT and mutant MD simulations yielded that VPA of the WT complex had slightly higher level of fluctuations, leading to a more flexible molecule compared with mutants (Figure 4B and 4C). This was an interesting observation, concluding that for a high affinity VPA binding, a certain level of flexibility of VPA might be a necessary event in VPA and WT CYP2C9 interactions.

At the next step, hydrogen bonding and hydrophobic contact analyses was conducted on the snapshots taken at 50$^{th}$ ns of MD simulations to validate the MM-PBSA based observation of occupied amino acids residues (Figure 5). LigPlot+ based screening of these interactions for the snapshots taken at 50$^{th}$ ns of MD simulations revealed that WT was using Ala103, His230, Leu233, Leu102, Phe114, Arg108, Glu104, Ala106, Arg105 and 5 water molecules to hold VPA (Figure 5A). Among these Arg105, Ala106 and a single water molecule was hydrogen bonded to VPA, whereas other molecules were all interacting through hydrophobic contacts (Figure 5A). Apart from Leu234 identified from MM-PBSA analyses (Figure 3B), Ligplot+ successfully validated MM-PBSA based predictions of amino acids contributing to the WT CYP2C9-VPA interaction. Albeit this validation, there were also other residues, not identified through MM-PBSA method that could be misrepresentative of the main contributors in WT CYP2C9-VPA interaction (Figure 5A). On the other hand, F114L has shown occupation of Asp293, Arg108, Val292 and 3 water molecules of which neither of them were identified though MM-PBSA analyses (Figure 5B). This indicated that without analyses of energetic contributions, Ligplot+ may return misleading information about interacting residues as in the case of F114L CYP2C9 and VPA. For I207T mutant, Asp293, Arg108, Val113, Ala297, Phe114, Phe100, Leu366, Gly296, Phe476, Leu208 and 2 water molecules were identified to be occupied at 50$^{th}$ ns (Figure 5C). All of the residues predicted through MM-PBSA for I207T were included in LigPlot+ analyses and all were using hydrophobic contacts (Figure 5C). However, there were additional residues that may bring ambiguous information on their potential contributions. Overall, while LigPlot+ analyses of interacting residues at 50$^{th}$ ns of MD

**Table 1**. Summary of MM-PBSA based estimation of relative binding energy between VPA and CYP2C9 structures

| Component | WT (AVG) | WT (SEM) | F114 (AVG) | F114 (SEM) | I207T (AVG) | I207T (SEM) |
|---|---|---|---|---|---|---|
| ΔE (VDWAALS) | -21.7 | 0.5 | -18.1 | 0.4 | -18.3 | 1.6 |
| ΔE (EEL) | -14.6 | 0.4 | -10.9 | 4.4 | -9.3 | 4.9 |
| ΔE (EPB) | 22.1 | 0.7 | 19.4 | 4.1 | 18.3 | 3.5 |
| ΔE (ENPOLAR) | -18.9 | 0.4 | -17.5 | 0.3 | -17.1 | 0.6 |
| ΔE (EDISPER) | 28.9 | 0.1 | 29.7 | 1.2 | 28.5 | 0.7 |
| ΔG (Gas) | -36.3 | 0.8 | -29.0 | 4.5 | -27.7 | 3.4 |
| ΔG (Solvation) | 32.1 | 0.4 | 31.6 | 5.0 | 29.6 | 3.4 |
| ΔG (Interaction) | -4.3 | 0.5 | 2.6 | 0.8 | 2.0 | 0.9 |

ΔE (VDWAALS): Van der Waals molecular mechanics energy, ΔE (EEL): Electrostatic molecular mechanics energy, ΔE (EPB): Polar contribution to the solvation energy, ΔE (ENPOLAR): Nonpolar contribution of repulsive solute-solvent interactions to the solvation energy, ΔE (EDISPER): Nonpolar contribution of attractive solute-solvent interactions to the solvation energy, ΔG (Gas): Total gas phase molecular mechanics energy, ΔG (Solvation): Total solvation energy, ΔG (Interaction): Total relative binding energy, AVG: Average, SEM: Standard error of the mean

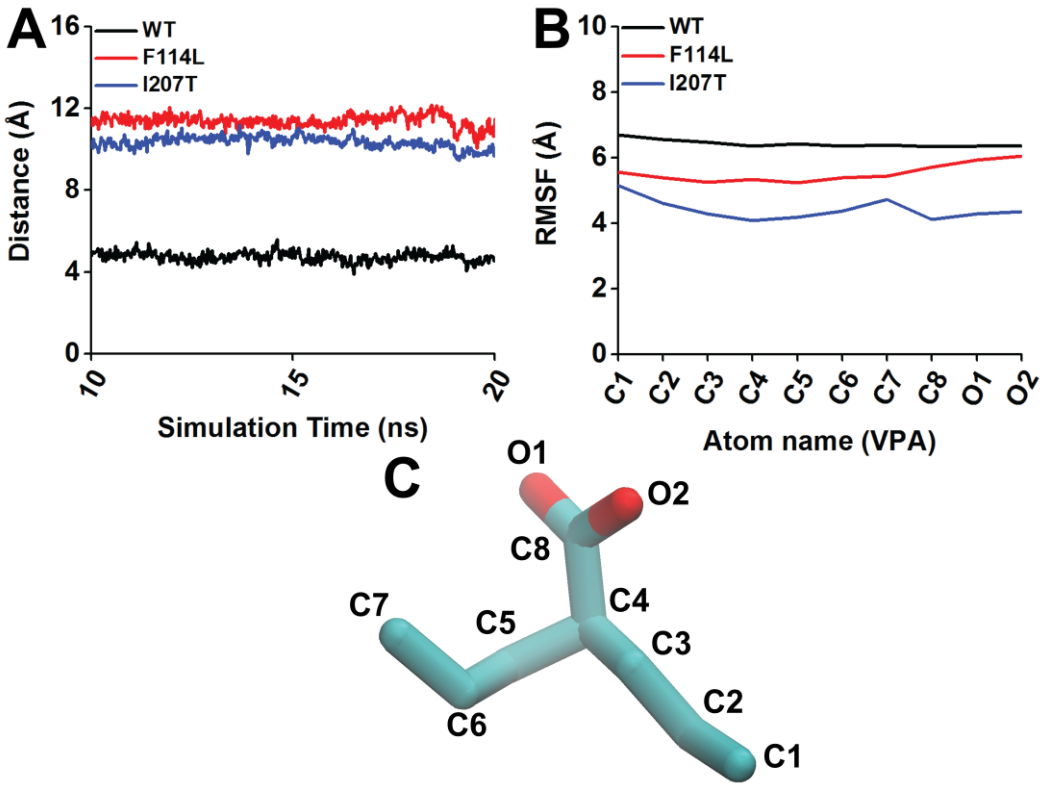


**Figure 4.** (A) Average distance between center of mass of Arg105 and Leu234 to the center of mass of VPA during last 40 ns of MD simulations were shown for WT and mutants. While WT complex maintained this distance around ~5 Å, mutant complexes remained almost 2 fold distant apart, validating the MM-PBSA observation obtained from last 10 ns of the simulations. (B) Average RMSF values, as an indicator of flexibility, were represented for VPA atoms in WT and mutant complexes for the last 40 ns of MD simulations. Interestingly, VPA had slightly higher RMSF values for each atom in WT compared with both of the mutants, demonstrating certain level of atomic fluctuations could be necessary to optimize VPA binding in higher affinity. (C) Atom naming used for VPA in (B).

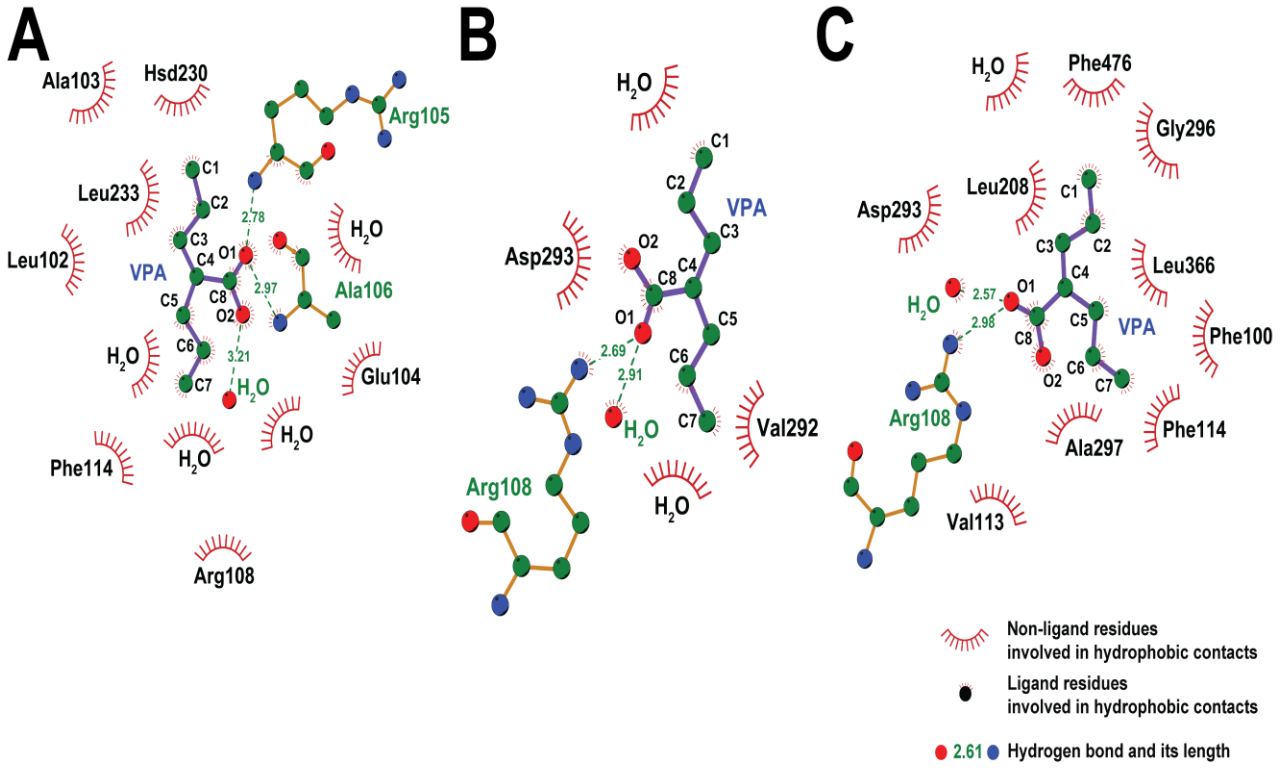


**Figure 5.** LigPlot+ based analyses of intermolecular interactions between WT CYP2C9 (A) and its mutants, F114L (B) and I207T (C) at the 50th ns of MD simulations. There was clear shift of occupied residues in mutants compared to WT.

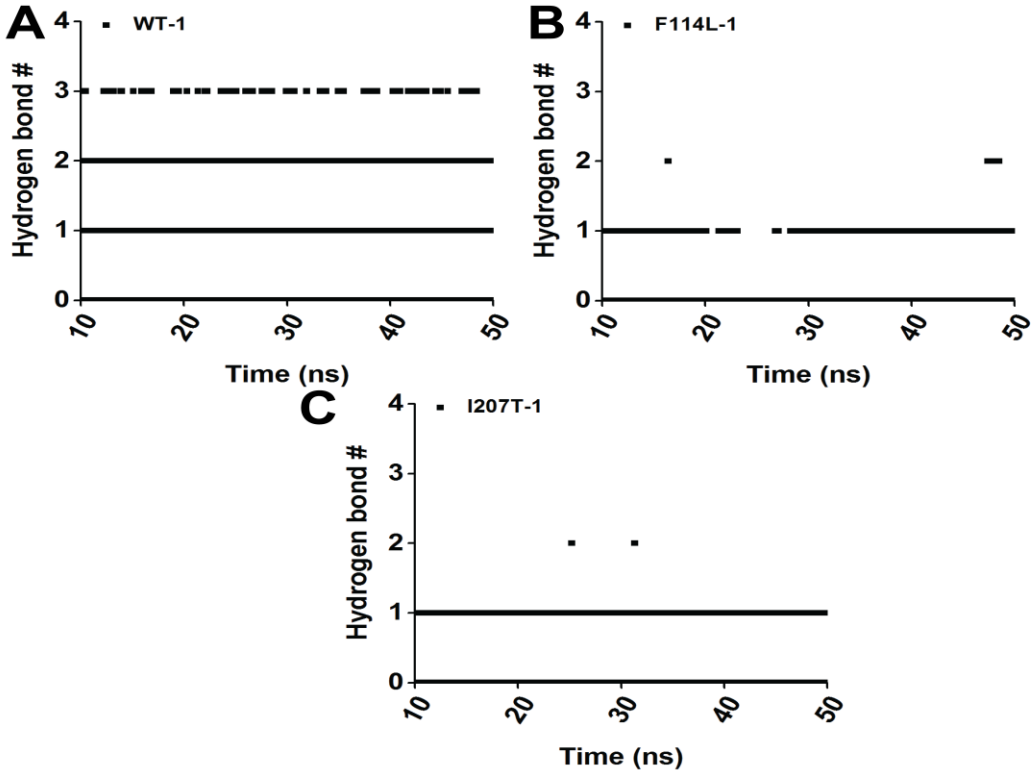


**Figure 6.** Number of hydrogen bonds between protein/heme and VPA during last 40 ns of MD simulations of WT (A) and its mutants, F114L (B) and I207T (C).

simulations validated the MM-PBSA residues for WT and I207T mutant, identification of additional residues was concluded to be unreliable. Hence, rather than implementing a LigPlot+ based static snapshot analyses, a more reliable temporal analyses of hydrogen bonding at the last 40 ns of all MD simulations were executed at the next step (Figure 6). At this point, both mutants seemed to lost most of the 2 and 3 hydrogen bond containing frames (Figure 6B and 6C) compared with WT (Figure 6A). These results on hydrogen bonding validated the overall ranking between WT and mutants in terms of MM-PBSA based prediction of relative binding energies.

## 4. Discussion and Conclusion

With this study, WT CYP2C9 and its mutants, F114L and I207T complexed with VPA were subjected to MD analyses and subsequent MM-PBSA based prediction of total relative binding energy and residue-wise amino acid contributions (Figure 2, 3 and Table 1). Based on these analyses, for the first time in literature, it was revealed that the mutations tested caused a significant decrease in relative binding energy compared to WT, through shifting occupied amino acid network involved in VPA binding. In addition, these observations were further supported by distance analyses (Figure 4A), RMSF based flexibility analyses (Figure 4B) LigPlot+ based interaction network analyses (Figure 5) and hydrogen bonding analyses (Figure 6). Overall, a clear shift of interaction network was documented for the first time in selected mutations through a computational approach.

One important limitation of this study was the exclusion of entropic contribution to the estimation of relative binding energy (Table 1). This approach was taken since a simple search in the literature returned many examples where entropy calculation were ignored or lacking due to misleading estimations [35-40]. Moreover, an entropy included MM-PBSA based prediction of the relative binding energy between WT CYP2C9 and VPA was found to be -5.05 kcal/mol of which is numerically very close to our entropy-less prediction, -4.3±0.5 kcal/mol (1.2 kcal/mol of difference) (Figure 3A and Table 1). While all these previous data support that omitted entropy calculations would not alter ranking of relative binding energy estimation in our case, it would be intriguing to see the entropy included results for all of the complexes.

Relative binding energy based ranking of CYP2C9 and its mutants towards VPA could be also interpreted as ranking of dissociation constants. However, strength of VPA binding to the enzymatic active site of CYP2C9 may not necessarily translate into changes in overall enzymatic activity. Thus when approaching MM-PBSA data, this caveat should be taken into account. Moreover, only under rapid equilibrium assumption of Michaelis-Menten kinetics, which states that the rate of substrate binding is faster than product formation, the dissociation constant would be equal to Km. However, this fact has been questioned in previous literature stating that most of the drug metabolizing cytochrome p450 enzymes do not follow Michelis-Menten kinetics and are classified as atypical enzymes [41]. Thus, this bottleneck has to be

considered when using the results obtained in this study.

The literature contains a single study in which CYP2C9 and VPA were analyzed with molecular dynamics simulations, followed by MM-GBSA based binding energy analyses [11]. In this paper, authors have evaluated average conformations of 50 ns MD simulations to extract important amino acids that were holding VPA in the enzymatic active site. These were concluded to be F100, R108, V113, F114, L201, N204, I205, L208, V292, G296, A297, E301 and F476. Due to fact that our approach was reliant on MM-PBSA based contribution of VPA interacting residues, Glu104, Arg105 and Ala106, Leu233 and Leu234 were identified for the WT, Arg97 and Val113 for F114L mutant and Val113, Ala 297, Leu266 and Phe476 for I207T mutant (Figure 3B). Based on these results, it was concluded that average structure based approach towards identification of VPA interacting residues may cover all possibilities, even though those residues do not reflect actual contribution to binding energy. This kind of potential misidentification of residues contributing to VPA interactions were also observed in the case which we have analyzed 50$^{th}$ ns frames via LigPlot+ (Figure 5). In sum, we believe that it is a more rational practice to allocate MM-PBSA based amino acid wise contributions to binding energy for ranking importance of residues towards binding.

CYP2C9 has been proposed to obey two-site binding model to hold multiple substrates simultaneously in its active site [42]. Our docked model of VPA in the CYP2C9 enzymatic active site only included one molecule, which may not reflect actual binding events within the binding site (Figure 1). Although VPA was docked as a single molecule, RMSF analyses of this molecule during last 40 ns of the simulation yielded higher flexibility of WT compared to both mutants (Figure 4B). These RMSF results may be deduced to the fact that because WT CYP2C0 has two functional binding sites in its active site, single VPA in the active site may have higher freedom. On the other hand, mutations introduced may possibly alter the structure of the active site leading to a more rigid VPA molecules. Although this perspective requires more detailed analyses via longer MD simulations, future studies may be designed to test this hypothesis.

In conclusion, here WT CYP2C9 and its two mutants F114L and I207T were analyzed by MD simulations and MM-PBSA based binding energetics, all of which yielded novel changes on the interaction network of amino acids upon these mutations. Hence, for the first time in literature, the amino acid wise alterations on how WT CYP2C9 loses its interaction capacity towards VPA upon these two mutations were reported. Future studies with more extensive characterization of binding energy will expand this knowledge further for CYP2C9 enzyme.

**Acknowledgment**

Molecular dynamics and MM-PBSA calculations described in this study were fully implemented at TUBITAK ULAKBIM, High Performance and Grid Computing Center (TRUBA resources).

**Declaration of Ethical Code**

*In this study, we undertake that all the rules required to be followed within the scope of the "Higher Education Institutions Scientific Research and Publication Ethics Directive" are complied with, and that none of the actions stated under the heading "Actions Against Scientific Research and Publication Ethics" are not carried out.*

**References**

[1] Chateauvieux, S., Morceau, F., Dicato, M., Diederich, M. 2010. Molecular and therapeutic potential and toxicity of valproic acid. Journal of Biomedicine and Biotechnology, 2010, 1-18.

[2] Ghodke-Puranik, Y., Thorn, C. F., Lamba, J. K., Leeder, J. S., Song, W., Birnbaum, A. K., Altman, R. B., Klein, T. E. 2013. Valproic acid pathway: pharmacokinetics and pharmacodynamics. Pharmacogenet Genomics, 23(4), 236-241.

[3] Terbach, N., Williams, R. S. 2009. Structure-function studies for the panacea, valproic acid. Biochemical Society Transactions, 37(5), 1126-1132.

[4] Leppik, I. E., Birnbaum, A. K. 2010. Epilepsy in the elderly. Annals of the New York Academy of Sciences, 1184, 208-224.

[5] Tan, L., Yu, J. T., Sun, Y. P., Ou, J. R., Song, J. H., Yu, Y. 2010. The influence of cytochrome oxidase CYP2A6, CYP2B6, and CYP2C9 polymorphisms on the plasma concentrations of valproic acid in epileptic patients. Clinical neurology and neurosurgery, 112(4), 320-323.

[6] Ito, M., Ikeda, Y., Arnez, J. G., Finocchiaro, G., Tanaka, K. 1990. The enzymatic basis for the metabolism and inhibitory effects of valproic acid: dehydrogenation of valproyl-CoA by 2-methyl-branched-chain acyl-CoA dehydrogenase. Biochimica et Biophysica Acta (BBA)-General Subjects, 1034(2), 213-218.

[7] Argikar, U. A., Remmel, R. P. 2009. Effect of aging on glucuronidation of valproic acid in human liver microsomes and the role of UDP-glucuronosyltransferase UGT1A4, UGT1A8, and UGT1A10. Drug Metabolism and Disposition, 37(1), 229-236.

[8] Sadeque, A. J., Fisher, M. B., Korzekwa, K. R., Gonzalez, F. J., Rettie, A. E. 1997. Human CYP2C9 and CYP2A6 mediate formation of the hepatotoxin 4-ene-valproic acid. Journal of Pharmacology and Experimental Therapeutics, 283(2), 698-703.

[9] Kiang, T. K., Ho, P. C., Anari, M. R., Tong, V., Abbott, F. S., Chang, T. K. 2006. Contribution of CYP2C9, CYP2A6, and CYP2B6 to valproic acid metabolism in hepatic microsomes from individuals with the CYP2C9*1/*1 genotype. Toxicological Sciences, 94(2), 261-271.

[10] Ho, P. C., Abbott, F. S., Zanger, U. M., Chang, T. K. 2003. Influence of CYP2C9 genotypes on the formation of a hepatotoxic metabolite of valproic acid in human liver microsomes. The Pharmacogenomics Journal, 3(6), 335-342.

[11] Bello, M., Mendieta-Wejebe, J. E., Correa-Basurto, J. 2014. Structural and energetic analysis to provide insight residues of CYP2C9, 2C11 and 2E1 involved in valproic acid dehydrogenation selectivity. Biochemical pharmacology, 90(2), 145-158.

[12] Daly, A. K., Rettie, A. E., Fowler, D. M., Miners, J. O. 2017. Pharmacogenomics of CYP2C9: Functional and Clinical Considerations. Journal of personalized medicine, 8(1), 1-31.

[13] Isvoran, A., Louet, M., Vladoiu, D. L., Craciun, D., Loriot, M. A., Villoutreix, B. O., Miteva, M. A. 2017. Pharmacogenomics of the cytochrome P450 2C family: impacts of amino acid variations on drug metabolism. Drug Discovery Today, 22(2), 366-376.

[14] Veronese, M. E., Miners, J. O., Rees, D. L., Birkett, D. J. 1993. Tolbutamide hydroxylation in humans: lack of bimodality in 106 healthy subjects. Pharmacogenetics, 3(2), 86-93.

[15] Zhang, H. F., Wang, H. H., Gao, N., Wei, J. Y., Tian, X., Zhao, Y., Fang, Y., Zhou, J., Wen, Q., Gao, J., Zhang, Y. J., Qian, X. H., Qiao, H. L. 2016. Physiological Content and Intrinsic Activities of 10 Cytochrome P450 Isoforms in Human Normal Liver Microsomes. Journal of Pharmacology and Experimental Therapeutics, 358(1), 83-93.

[16] Webb, B., Sali, A. 2016. Comparative Protein Structure Modeling Using MODELLER. Current protocols in bioinformatics, 15(1), 5-6.

[17] Humphrey, W., Dalke, A., Schulten, K. 1996. VMD: visual molecular dynamics. Journal of Molecular Graphics, 14(1), 33-38.

[18] Trott, O., Olson, A. J. 2010. AutoDock Vina: improving the speed and accuracy of docking with a new scoring function, efficient optimization, and multithreading. Journal of Computational Chemistry, 31(2), 455-461.

[19] Vanommeslaeghe, K., MacKerell, A. D., Jr. 2012. Automation of the CHARMM General Force Field (CGenFF) I: bond perception and atom typing. Journal of Chemical Information and Modeling, 52(12), 3144-3154.

[20] Vanommeslaeghe, K., Raman, E. P., MacKerell, A. D., Jr. 2012. Automation of the CHARMM General Force Field (CGenFF) II: assignment of bonded parameters and partial atomic charges. Journal of Chemical Information and Modeling, 52(12), 3155-3168.

[21] Best, R. B., Zhu, X., Shim, J., Lopes, P. E., Mittal, J., Feig, M., Mackerell, A. D., Jr. 2012. Optimization of the additive CHARMM all-atom protein force field targeting improved sampling of the backbone phi, psi and side-chain chi(1) and chi(2) dihedral angles. Journal of Chemical Theory and Computation, 8(9), 3257-3273.

[22] Huang, J., Rauscher, S., Nawrocki, G., Ran, T., Feig, M., de Groot, B. L., Grubmuller, H., MacKerell, A. D., Jr. 2017. CHARMM36m: an improved force field for folded and intrinsically disordered proteins. Nature Methods, 14(1), 71-73.

[23] MacKerell, A. D., Bashford, D., Bellott, M., Dunbrack, R. L., Evanseck, J. D., Field, M. J., Fischer, S., Gao, J., Guo, H., Ha, S., Joseph-McCarthy, D., Kuchnir, L., Kuczera, K., Lau, F. T., Mattos, C., Michnick, S., Ngo, T., Nguyen, D. T., Prodhom, B., Reiher, W. E., Roux, B., Schlenkrich, M., Smith, J. C., Stote, R., Straub, J., Watanabe, M., Wiorkiewicz-Kuczera, J., Yin, D., Karplus, M. 1998. All-atom empirical potential for molecular modeling and dynamics studies of proteins. The Journal of Physical Chemistry B, 102(18), 3586-3616.

[24] Mackerell, A. D., Jr., Feig, M., Brooks, C. L. 2004. Extending the treatment of backbone energetics in protein force fields: limitations of gas-phase quantum mechanics in reproducing protein conformational distributions in molecular dynamics simulations. Journal of Computational Chemistry, 25(11), 1400-1415.

[25] Jorgensen, W. L., Madura, J. D. 1983. Quantum and statistical mechanical studies of liquids. 25. Solvation and conformation of methanol in water. Journal of the American Chemical Society, 105(6), 1407-1413.

[26] Martyna, G. J., Hughes, A., Tuckerman, M. E. 1999. Molecular dynamics algorithms for path integrals at constant pressure. Journal of Chemical Physics, 110(7), 3275-3290.

[27] Feller, S. E., Zhang, Y. H., Pastor, R. W., Brooks, B. R. 1995. Constant-Pressure Molecular-Dynamics Simulation - the Langevin Piston Method. Journal of Chemical Physics, 103(11), 4613-4621.

[28] Hoover, W. G. 1985. Canonical dynamics: Equilibrium phase-space distributions. Physical Review A, 31(3), 1695-1697.

[29] Wallace, A. C., Laskowski, R. A., Thornton, J. M. 1995. LIGPLOT: a program to generate schematic diagrams of protein-ligand interactions. Protein Engineering, Design and Selection, 8(2), 127-134.

[30] Miller, B. R., McGee, T. D., Jr., Swails, J. M., Homeyer, N., Gohlke, H., Roitberg, A. E. 2012. MMPBSA.py: An Efficient Program for End-State Free Energy Calculations. Journal of Chemical Theory and Computation, 8(9), 3314-3321.

[31] Berman, H. M., Westbrook, J., Feng, Z., Gilliland, G., Bhat, T. N., Weissig, H., Shindyalov, I. N., Bourne, P. E. 2000. The Protein Data Bank. Nucleic acids research, 28(1), 235-242.

[32] Wester, M. R., Yano, J. K., Schoch, G. A., Yang, C., Griffin, K. J., Stout, C. D., Johnson, E. F. 2004. The structure of human cytochrome P450 2C9 complexed with flurbiprofen at 2.0-A resolution. Journal of Biological Chemistry, 279(34), 35630-35637.

[33] Dai, D. P., Xu, R. A., Hu, L. M., Wang, S. H., Geng, P. W., Yang, J. F., Yang, L. P., Qian, J. C., Wang, Z. S., Zhu, G. H., Zhang, X. H., Ge, R. S., Hu, G. X., Cai, J. P. 2014. CYP2C9 polymorphism analysis in Han Chinese populations: building the largest allele frequency database. The Pharmacogenomics Journal,, 14(1), 85-92.,

[34] Tracy, T. S., Hutzler, J. M., Haining, R. L., Rettie, A. E., Hummel, M. A., Dickmann, L. J. 2002. Polymorphic variants (CYP2C9*3 and CYP2C9*5) and the F114L active site mutation of CYP2C9: effect on atypical kinetic metabolism profiles. Drug Metabolism and Disposition, 30(4), 385-390.

[35] Genheden, S., Ryde, U. 2015. The MM/PBSA and MM/GBSA methods to estimate ligand-binding affinities. Expert Opinion on Drug Discovery, 10(5), 449-461.

[36] Spackova, N., Cheatham, T. E., 3rd, Ryjacek, F., Lankas, F., Van Meervelt, L., Hobza, P., Sponer, J. 2003. Molecular dynamics simulations and thermodynamics analysis of DNA-drug complexes. Minor groove binding between 4',6-diamidino-2-phenylindole and DNA duplexes in solution. Journal of the American Chemical Society, 125(7), 1759-1769.

[37] Yang, T., Wu, J. C., Yan, C., Wang, Y., Luo, R., Gonzales, M. B., Dalby, K. N., Ren, P. 2011. Virtual screening using molecular simulations. Proteins, 79(6), 1940-1951.

[38] Foloppe, N., Hubbard, R. 2006. Towards predictive ligand design with free-energy based computational methods? Current Medicinal Chemistry, 13(29), 3583-3608.

[39] Wang, J. M., Hou, T. J., Xu, X. J. 2006. Recent Advances in Free Energy Calculations with a Combination of Molecular Mechanics and Continuum Models. Current Computer-Aided Drug Design, 2(3), 287-306.

[40] Homeyer, N., Gohlke, H. 2012. Free Energy Calculations by the Molecular Mechanics Poisson-Boltzmann Surface Area Method. Molecular Informatics, 31(2), 114-122.

[41] Atkins, W. M. 2005. Non-Michaelis-Menten kinetics in cytochrome P450-catalyzed reactions. Annual Review of Pharmacology and Toxicology, 45 291-310.

[42] Hutzler, J. M., Hauer, M. J., Tracy, T. S. 2001. Dapsone activation of CYP2C9-mediated metabolism: evidence for activation of multiple substrates and a two-site model. Drug Metabolism and Disposition, 29(7), 1029-1034.